Stability of Two-Dimensional Perovksites

Dino Đudarić[*]

Department of Physics, Faculty of Science, Bijenička 32, Zagreb

Advisor: Luca Grisanti

Division of Theoretical Physics, Ruđer Bošković Institute, Bijenička cesta 54, Zagreb

(Dated: January 23, 2022)

We studied stability of 2D and 3D pervoskites to oxygen and light induced superoxide through DFT calculations of reaction energy.

I. INTRODUCTION

Hybrid inorganic-organic halide perovskite are a promising class of materials for development of low-cost optoelectronic devices such as solar cells, light-emitting diodes and lasers. Solar cell application in particular have attracted intense interest in recent years with rapid rise in power conversion efficiencies of up to 22% for perovskite photovoltaics[1]. Perovskite materials share similar structural features with the namesake mineral $CaTiO_3$. The structure of methylammonium lead iodide, $CH_3NH_3PbI_3$ (or $MAPbI_3$) is shown on Figure 1. As can be seen Methylammonium cation ($CH_3NH_3^+$) occupies the central site surrounded by 12 nearest-neighbour iodide ions in corner-sharing PbI_6 octahedra. Many interesting properties of halide perovskites derive form their soft lattices and dynamically disordered crystal structure, which favorably modifies their charge-carrier recombination lifetimes.[2] However, a major obstacle in further development exists in the form of limited composition accessibility in the ABX_3 (A $= Cs^+$, $CH_3NH_3^+$, $[HC(NH_2)_2]^+$; B $= Pb^{2+}$, Ge^{2+}, Sn^{2+}; X $= Cl^-$, Br^-, I^-) perovskite structure, with only three A-site cations being able to maintain the 3D corner-sharing inorganic framework, in some cases forming only metastable compounds. Solution to this compositional diversity was found in the form of two-dimensional halide perovskites.[2]

2D perovskites accomplished through chemical dimensional reduction of 3D crystal lattice, $(A')_m(A)_{n-1}B_nX_{3n+1}$, adopt a new structural and compositional dimension, where monovalent (m = 2) or divalent (m = 1) A' cations can intercalate between the anions of the 2D perovskite sheets. This offers variety of hybrid organic-inorganic materials with tailorable functionalities but also give rise to an unparalleled structural complexity which allows for the fine-tuning of the optoelectronic properties. Figure 2. shows the structure of 2D perovskites with different number of layers n and their comparison to 3D perovskite. In the 2D hybrid halide perovskites, the organic cations act as insulating barriers that confine the charge carriers in two dimensions, but they also serve as dielectric moderators

that determine the electrostatic forces exerted on the photogenerated electron-hole pairs.[2]
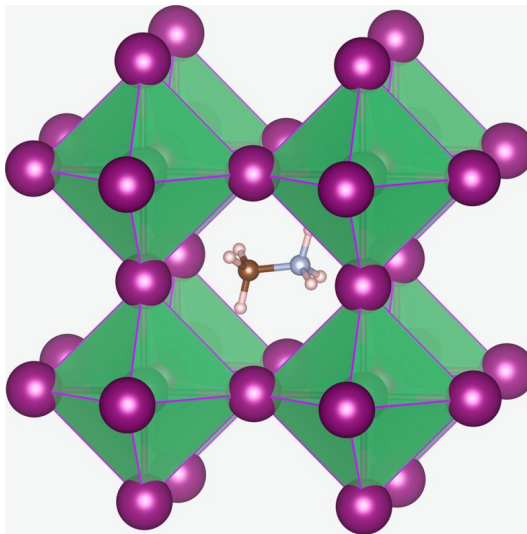
Figure 1. Structure of 3D perovskite $MAPbI_3$.[3]

Before halide perovskites can be successfully used in commercial solar cell applications long term stability needs to be studied. It has been generally observed that external conditions such as moisture, elevated temperature, oxygen and UV radiation, all cause device instability at higher rates than those typically observed in polymer and dye-sensitized photovoltaics. Possible solution to stability issues would be use of 2D perovskites with similar power conversion efficiencies.
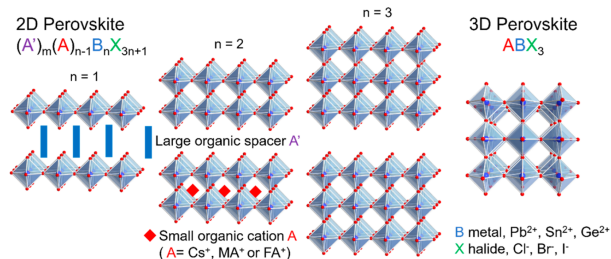
Figure 2. Schematic illustration of the evolution from 2D perovskite to 3D perovskite with key components.[2]

[*] djudaric.phy@pmf.hr

Inspired by recent work[1,4], we have here decided to calculate reaction energies of 3D and 2D Perovskites with i) neutral oxygen O_2 and ii) the superoxide ion O_2^-, a reactive species produced in the photoionization induced by the light. We have employed DFT as a computational technique to evaluate the energy of reactant and products and so estimate the reaction energy.

II. DENSITY FUNCTIONAL THEORY

Density functional theory was originally formulated by Kohn in two works: providing the theoretical background[5] and the instructions for DFT calculations[6]. The key theoretical concepts develop around the idea that an external potential U in which particles are moving is uniquely determined (up to a constant) by the density of particles $n(\vec{r})$ in the ground state and the system energy $E[n]$ is a functional of particle density $n(\vec{r})$, while the ground state energy is a global minimum of this functional and particle density of this global minimum is the ground state particle density[5]. The exact particle density of the system, $n(\vec{r})$, can be viewed as particle density of fictitious system (the "Kohn-Sham system") of non-interacting particles[6]. Besides, any Kohn-Sham non-interacting particle is moving in non local Kohn-Sham potential, V_{KS}, which has multiple contributions: U external potential, V_H Hartree potential (Coulomb potential of other particles) and potential of exchange and correlation V_{xc}. V_{xc} is generally a non-local contribution, is the most critical part of density functional theory as its form is unknown so varying approximations are used. For exchange part of V_{xc}, Hartree-Fock exchange gives exact values however since it is non-local contribution it is numerically demanding so it is replaced by approximations like Dirac LDA (local density approximation), GGA (generalized gradient approximation), hybrid potential (mix of HF and local potentials), etc. For correlation part of V_{xc} approximations are constructed by interpolating analytical calculations (perturbation theory) and adjusting numerical results. Considering all this we get Schrödinger equation for Kohn-Sham particles:

$$\left[-\frac{\hbar^2}{2m} \vec{\nabla}^2 + U(\vec{r}) + V_H(\vec{r}) \right] \psi_m(\vec{r})$$
$$+ \int d\vec{r'} V_{xc}(\vec{r'}, \vec{r}) \psi_m(\vec{r'}) = e_m \psi_m(\vec{r}) \quad (1)$$

which is 3-dimensional partial differential equation. The density of Kohn-Sham particles (and exact density) in the ground state can be calculated from wave functions:

$$n(\vec{r}) = \sum_{\substack{occupied \\ states}} |\psi_n(\vec{r})|^2 \quad (2)$$

Kohn-Sham potential depends on particle density so potentials, density and wave functions need to be calculated self-consistently.

In this work DFT calculations are performed with Quantum Espresso[7,8] (QE) program suite, which has various routines used for calculations, analysis of calculated data or their graphical display. QE uses plane wave basis for representing Bloch wave functions. For periodic part of Bloch wave function, Fourier series of reciprocal lattice vectors is used. Considering numerical restrictions, Fourier series is truncated for sufficiently high wave number. Then, solving the Schrödinger equation comes down to determining eigenvalues of matrix with eigenvectors built from Fourier components of wave function. The problem is solved in a self-consistent fashion, through a set of cycles of self-consistent field (SCF). As in common implementation not all particles are treated individually, the problem of movement of all electrons is simplified by considering only valence electrons. Kohn-Sham potential of nucleus with core electrons is replaced by effective potential called pseudopotential. There are many different pseudopotentials generated with different specifications and approximations. The pseudopotentials used in all our calculations are ultrasoft GGA-PBE (generalized gradient approximation)[9] with nonlinear core correction. The functional used is 'vdW-DF-cx'[10,11] which stands for *van der Waals density functional with consistent exchange*. It is important to use same pseudopotentials and functional in all calculation to get comparable results.

Routines used in our calculations are 'relax' and 'vc-relax'. In 'relax' routine, QE calculates forces on each atom and moves (relaxes) the atoms towards a configuration with smaller forces and lower energy using Broyden–Fletcher–Goldfarb–Shanno (BFGS) algorithm. Each step in BFGS algorithm involves self-consistent solution to equation (1). Vc in 'vc-relax' stands for *variable cell* so along atom positions cell parameters are also optimized. These routines are used to relax bulk structures however relaxing isolated molecules is also possible by using large unit cells so that interaction between cells is avoided.
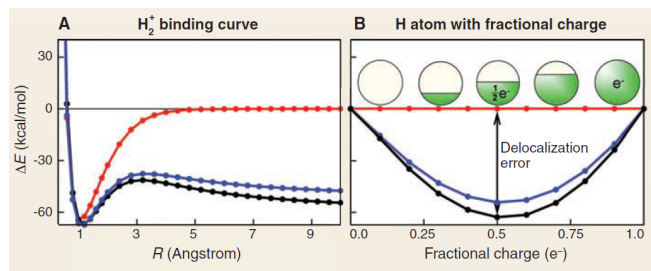
Figure 3. Illustration of delocalization error[12]

An important aspect to be aware when running DFT calculations, especially with charged molecules, is the delocalization error[12]. The exact energy of the atom as a function of charge is a straight-line interpolation between the integers, because of the discrete nature of electrons. However, approximate DFT functionals are incorrectly convex between the integers and they predict an energy

that is too low for fractional charges. Figure 3. illustrates the problem with H_2^+ molecule[12], a system that contains a single electron. Although DFT gives good bonding structures, errors increase with bond length. The huge discrepancies at dissociation energy of H_2^+ exactly match the error of the atoms with fractional charges (Figure 3.). Stretched H_2^+ clearly shows that the energy is too low if the electron is delocalized over the two centers. This is a consequence of the delocalization error, which refers to the tendency of approximate functionals to spread out the electron density artificially. We directly experienced this problem in our calculations, where delocalization error affects the SCF convergence of superoxide (O_2^-) ion (see below).

III. RESULTS AND DISCUSSION

III.1. Calculation of reaction energies

Reaction energy E_R is calculated as energy difference between products and reactants:

$$E_R = \sum_{products} E - \sum_{reactants} E \qquad (3)$$

Energies of reactants and products are obtained by relaxing their structures. For each of them, a *reference state* has to be chosen - a choice that can carry a degree of arbitrariness. O_2, H_2O, X_2 and alkylamines are assumed to be isolated molecule and then are relaxed in large cells (much larger than distance between atoms) which corresponds to gas state. On the other side, perovskites and lead halide (PbX_2) are relaxed in their crystal lattices which corresponds to solid state.
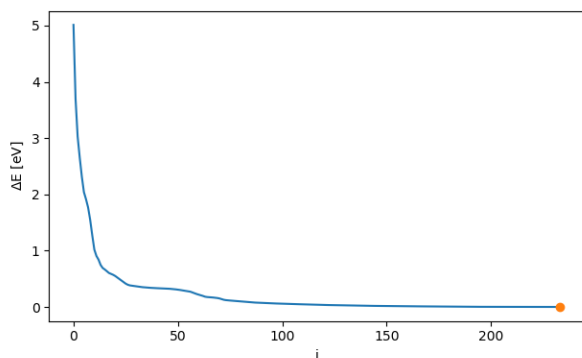
Figure 4. Energy difference between final energy and energy on each step of BFGS geometry optimization for MAPbI3.

Figure 4. shows how 'vc-relax' routine finds minimum energy for MAPbI3 lattice. ΔE is difference between energy on i step of BFGS geometry optimization and final energy. Energy difference is smaller by each step until convergence threshold is reached.

III.2. Reaction with 3D Perovskites

Reaction energies for methylammonium lead halide ($CH_3NH_3PbX_3$ or $MAPbX_3$) 3D perovskites in reaction with oxygen is calculated for bromide and iodide (X = Br, I) using following chemical reaction:

$$4CH_3NH_3PbX_3+O_2\rightarrow4PbX_2+2X_2+2H_2O+4CH_3NH_2 \qquad (4)$$
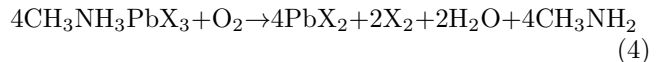
In this reaction O_2, X_2, H_2O and CH_3NH_2 are in gas state, while $CH_3NH_3PbX_3$ and $4PbX_2$ are in solid state. For MAPbBr3 perovskite, reaction energy of $E_R=7.08$ eV is obtained. And for MAPbI3 perovskite, reaction energy of $E_R=4.60$ eV is obtained. These values indicate that degradation process in the absence of light is unfavorable. This is consistent with experimental observation[4]. Also the relation between results, larger for MAPbBr3 than MAPbI3 is consistent with experimental observations of longer operational lifetimes of MAPbBr3 than MAPbI3.[4]. However obtained values don't match previously calculated values[4]. They obtained values of 1.56 eV for MAPbI3 and 4.98 eV for MAPbBr3. The small differences in the computational set-up (e.g. code employed, pseudopotentials, etc.) cannot justify such large differences. We inquired the authors of Ref. 4 to understand the origin of the discrepancy, and it seems that they have placed the molecule in the bulk material, providing a reference state that is less stable and so more prone to react. In other words, in this calculation we didn't consider the effect of oxygen diffusion in bulk material. To get comparable result it is necessary to calculate energy of oxygen molecule placed inside MAPbX3 perovskite structure. This step is promoted by the presence of light.
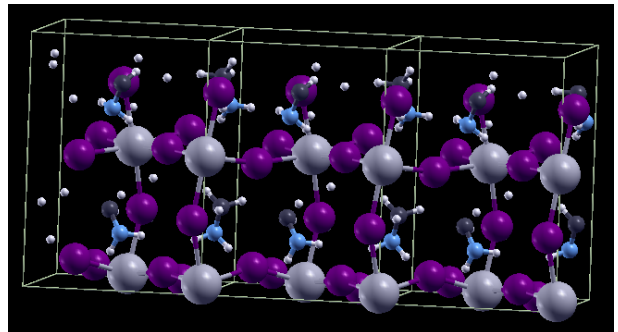
Figure 5. MAPbI$_3$ relaxed structure. Some of the organic molecules are broken across periodic images.

Figure 5. shows relaxed structure of MAPbI$_3$. As can be seen octahedra of the inorganic structure and methylammonium cations are slightly tilted from ideal structure seen in Figure 1. This is a natural result of 'vc-relax' routine which found that this tilted configuration minimizes energy.

The presence of light leads ultimately to a reaction of

photo-oxidized $CH_3NH_3PbX_3^*$ with superoxide O_2^-:

$$4CH_3NH_3PbX_3^* + O_2^- \rightarrow 4PbX_2 + 2X_2 + 2H_2O + 4CH_3NH_2 \tag{5}$$
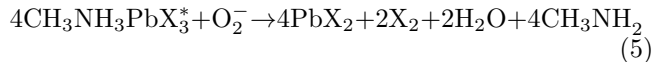
In this reaction photo-oxidized $CH_3NH_3PbI_3^*$ is calculated using 2x2x1 supercell, cell with 4 $CH_3NH_3PbI_3$ formula units and one electron missing from the system. Photo-oxidized $CH_3NH_3PbBr_3^*$ was relaxed using 2x2x2 supercell, cell with 8 $CH_3NH_3PbBr_3$ formula units and two missing electrons from the system. With calculation of isolated O_2^- superoxide we encountered problem of convergence which is due to delocalization error. O_2^- ion is a molecule with an odd number of electrons where the particular electronic configuration of molecular oxygen magnifies this issue. To induce localization and enforce the correct electronic state, we came to the solution of relaxing O_2^- molecule in presence of a dielectric environment. In QE this can be obtained with continuum solvation module *environ*, and selecting water as solvent. Relaxed O_2^- structure obtained from the calculation in water has been then transferred in vacuum and reconverged to get the correct energy, by using that electronic density as a starting guess.

All other molecules are relaxed as described for previous reaction. Reaction energy of E_R=9.88 eV is obtained for MAPbBr$_3^*$ and E_R=7.36 eV for MAPbI$_3^*$. These values are contradicting expectation of lower stability for reaction in presence of light. Compared to values from the same work in the literature[4], also calculated using DFT, of -1.39 eV for MAPbI$_3$ and 2.00 eV for MAPbBr$_3$, our result appears to be off. However this deviation can be explained by differing approaches, our approach considers reaction of gas superoxide separated from bulk while approach in cited paper is relaxation of oxygen diffused in bulk material. We probably operate a wrong choice of the reference state for the reactant. Initially we were hoping to reproduce their results for 3D perovskites and apply same approach to 2D perovskites. This suggests the need for future calculation of oxygen placed in bulk structure which should possibly replicate the mentioned results. In parallel, it may be important to consider vacancies for photo-degradation of organic-inorganic lead halide perovksites. Unfortunately the description in the work of Ref. 4 is not so clear. We are in contact with the authors to precisely understand which where their assumptions.

III.3. Reaction with 2D Perovskites

For 2D perovskite we calculated reaction energy of butylamonium lead halide $(BAH)_2PbX_4$ with oxygen where halide is bromide or iodide (X = Br, I):

$$2(BAH)_2PbX_4 + O_2 \rightarrow 2PbX_2 + 2X_2 + 2H_2O + 4BA \tag{6}$$

In this reaction BA, O_2, X_2 and H_2O are in gas state, while $(BAH)_2PbX_4$ and PbX_2 are in solid state. Values obtained are E_R=8.07 eV for bromide 2D perovskite

and E_R=5.83 eV for iodide 2D perovskite. Comparing to their 3D counterparts for bromide perovskite we have a difference of ΔE_R=0.99 eV and for iodide perovskite difference of ΔE_R=1.23 eV. This indicates improved stability of 2D perovskite compared to 3D perovskite. However it will be necessary to also calculate reaction energy for reaction with superoxide and also reaction energy for oxygen and superoxide infused in structures.
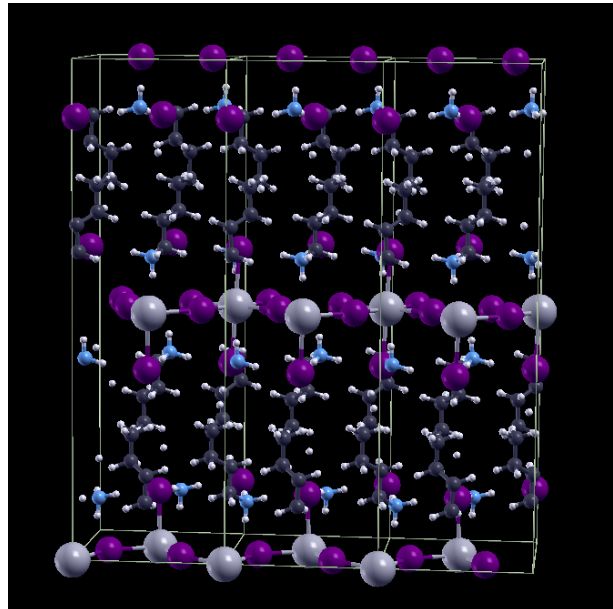
Figure 6. $(BAH)_2PbI_4$ relaxed structure.

Figure 6. shows relaxed structure of $(BAH)_2PbX_4$ 2D perovskite. This is a n=1 2D perovskite, there is 1 layer of inorganic perovskite structure. Comparing to 3D perovskite we can see big difference obtained by switching organic cations. Butylamine acts as spacer between inorganic layers, while methylammonium rests inside inorganic structure. Figure 7. shows difference between methylammonium and butylamine 3D structures. Except size difference butylamine has more conformation freedom (some of the bond can flip) and hence it can "squeeze" in some extent.
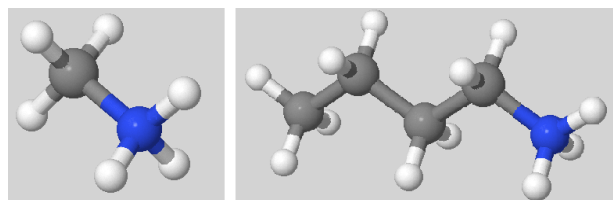
Figure 7. Molecular cations: methylammonium (left) and butylamine (right). White hydrogen, gray carbon, blue nitrogen.

IV. CONCLUSION

We have calculated reaction energy for 3D perovskites $MAPbI_3$ and $MAPbBr_3$ with oxygen for reaction (4). Obtained values are consistent with experimental observation of longer operational lifetimes of $MAPbI_3$ than $MAPbBr_3$. However computed values differ form ones computed by another group. This necessitates further calculations with different reactant state to confirm source of deviation of computed values. We have also calculated reaction energy for photo-oxidized 3D perovskite $MAPbI_3^*$ and $MAPbBr_3^*$ in reaction with superoxide (5). Similarly here is also discrepancy between obtained values which also suggest the need of a different reactant state and a better understanding of the light-induced reaction steps. Finally we have calculated reaction energy of 2D perovskites $(BAH)_2PbI_4$ and $(BAH)_2PbBr_4$ with oxygen for reaction (6). Obtained values coincide with expectation of increased stability to oxygen of 2D perovskite compared to 3D perovskite. Further calculations of oxygen and superoxide infused in structures of 2D and 3D perovskites will allow to have a insight to stability of 2D perovskites to oxygen.

V. ACKNOWLEDGMENTS

[1] Aristidou, N., Eames, C., Sanchez-Molina, I. et al. Fast oxygen diffusion and iodide defects mediate oxygen-induced degradation of perovskite solar cells. Nat Commun 8, 15218 (2017).

[2] J. Am. Chem. Soc. 2019, 141, 1171-1190

[3] Eames C, Frost JM, Barnes PR, O'Regan BC, Walsh A, Islam MS. Ionic transport in hybrid lead iodide perovskite solar cells. Nat Commun. 2015 Jun 24;6:7497. doi: 10.1038/ncomms8497. PMID: 26105623; PMCID: PMC4491179.

[4] Chem. Mater. 2020, 32, 1, 400–409

[5] Hohenberg P, Kohn W (1964) Phys Rev B 136:B864–B871

[6] Kohn W, Sham LJ (1965) Phys Rev 140:1133–1138

[7] P. Giannozzi et al., J.Phys.:Condens.Matter 21, 395502 (2009)

[8] P. Giannozzi et al., J.Phys.:Condens.Matter 29, 465901 (2017)

[9] J.P. Perdew, K. Burke & M. Ernzerhof, Phys. Rev. Lett. 78 (1996) 1396

[10] T. Thonhauser et al., PRL 115, 136402 (2015).

[11] T. Thonhauser et al., PRB 76, 125112 (2007).

[12] A. J. Cohen, P. Mori-Sanchez, W. Yang, Science 321, 792 (2008).